HHS Public Access

Author manuscript

Dev Biol. Author manuscript; available in PMC 2024 April 01.

Published in final edited form as:

Dev Biol. 2023 April ; 496: 1–14. doi:10.1016/j.ydbio.2023.01.003.

Zebrafish *her3* knockout impacts developmental and cancer-related gene signatures

Matthew R. Kent[1], **Delia Calderon**[1,2], **Katherine M. Silvius**[1], **Jack P. Kucinski**[1,2], **Collette A. LaVigne**[3], **Matthew V. Cannon**[1], **Genevieve C. Kendall**[1,2,4,#]

[1]Center for Childhood Cancer & Blood Diseases, The Abigail Wexner Research Institute, Nationwide Children's Hospital, Columbus, OH 43205, USA.

[2]Molecular, Cellular, and Developmental Biology Ph.D. Program, The Ohio State University, Columbus, OH 43210, USA.

[3]Department of Molecular Biology, UT Southwestern Medical Center, Dallas, TX 75390, USA.

[4]Department of Pediatrics, The Ohio State University College of Medicine, Columbus, OH 43205, USA.

Abstract

HES3 is a basic helix-loop-helix transcription factor that regulates neural stem cell renewal during development. *HES3* overexpression is predictive of reduced overall survival in patients with fusion-positive rhabdomyosarcoma, a pediatric cancer that resembles immature and undifferentiated skeletal muscle. However, the mechanisms of *HES3* cooperation in fusion-positive rhabdomyosarcoma are unclear and are likely related to *her3*/*HES3's* role in neurogenesis. To investigate *HES3's* function during development, we generated a zebrafish CRISPR/Cas9 null mutation of *her3*, the zebrafish ortholog of *HES3*. Loss of *her3* is not embryonic lethal and adults exhibit expected Mendelian ratios. Embryonic *her3* zebrafish mutants exhibit dysregulated *neurog1* expression, a *her3* target gene, and the mutant *her3* fails to bind the *neurog1* promoter sequence. Further, *her3* mutants are significantly smaller than wildtype and a subset present with lens defects as adults. Transcriptomic analysis of *her3* mutant embryos indicates that genes involved in organ development, such as *pctp and grinab,* are significantly downregulated. Further, differentially expressed genes in *her3* null mutant embryos are enriched for Hox and Sox10 motifs. Several cancer-related gene pathways are impacted, including the inhibition of matrix metalloproteinases. Altogether, this new model is a powerful system to study *her3/HES3*-mediated neural development and its misappropriation in cancer contexts.

[#]Author for Correspondence: Genevieve.Kendall@NationwideChildrens.org.

Author Contributions

Conceptualization: M.K., G.K.; Methodology: M.K., C.L., G.K.; Software: M.C.; Validation: M.K., M.C., G.K.; Formal analysis: M.K., D.C., J.K., M.C., G.K.; Investigation: M.K., D.C., K.S., J.K., C.L., G.K.; Resources: G.K.; Data Curation: M.C., G.K.; Writing – original draft: M.K., M.C., G.K.; Writing – review and editing: M.K., D.C., K.S., J.K., C.L., M.C., G.K.; Visualization: M.K., M.C., G.K.; Supervision: G.K.; Project administration: G.K.; Funding acquisition: G.K.

Competing Interests

The authors declare no competing or financial interests.

Graphical Abstract

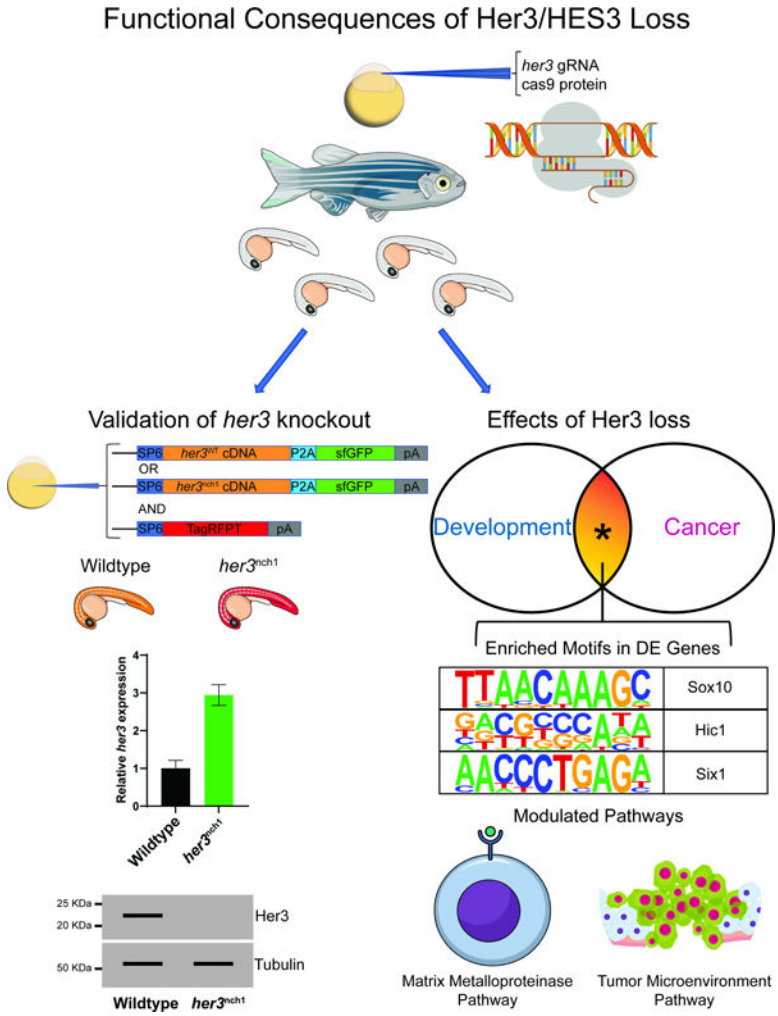

Keywords

Her3/HES3; functional genomics; zebrafish; CRISPR/Cas9 knockout; neural development; transcriptomics

Introduction

HES3, and the zebrafish ortholog *her3*, are part of the *HES* gene family, a group of basic helix-loop-helix transcriptional repressors (Sasai et al., 1992). There are seven *HES* family genes that are conserved between humans and mice, in addition to *HES4,* which contains no mouse ortholog. In zebrafish, there are 13 *her* genes that are orthologs to the mammalian *HES* genes: *her6* is orthologous to *HES1*; *her3* is orthologous to *HES3*; *her9* to *HES4*; *her2*, *her4.1*, *her12*, and *her15* to *HES5*; *her8a* and *her13* to *HES6*; and *her1*, *her5*, *her7,* and *her11* to *HES7* (Davis and Turner, 2001, El Yakoubi et al., 2012, Sieger et al., 2004, Shankaran et al., 2007, Sieger et al., 2006, Gajewski and Voolstra,

2002). A subset of the *HES* family is known to regulate neurogenesis, such as *Hes1, Hes3,* and *Hes5* (Ohtsuka et al., 1999, Hirata et al., 2001, Hatakeyama et al., 2004). These data originated from a *Hes1/Hes3* double knock-out mouse, in which neural progenitor cells in the midbrain and anterior hindbrain prematurely differentiated, preventing these areas from fully developing (Hirata et al., 2001). In mouse and rat neural stem cells, *Hes3* functions in a non-canonical Notch signaling pathway. This pathway is mediated through soluble Notch ligands which bind to Notch receptors, thus activating kinases to phosphorylate serine-727 on Stat3, and ultimately resulting in an upregulation of *Hes3* and self-renewal of neural stem cells (Artavanis-Tsakonas et al., 1999, Androutsellis-Theotokis et al., 2006, Androutsellis-Theotokis et al., 2009, Kageyama et al., 2008, Hans et al., 2004, Bae et al., 2005).

Other *HES* family genes are responsible for segmentation of somites in mice, bilateral structures on either side of the neural tube that give rise to vertebrae, ribs, and skeletal muscle as examples (Dubrulle and Pourquie, 2004). Cyclic expression of *Hes1, Hes5*, and *Hes7* in mice, and *her1* and *her7* in zebrafish, are responsible for the segmentation of somites (Jouve et al., 2000, Dunwoodie et al., 2002, Bessho et al., 2001a, Bessho et al., 2001b, Muller et al., 1996, Holley et al., 2002, Oates and Ho, 2002). This is a tightly regulated developmental process, as cyclical expression of *Hes7* is critical for somite segmentation, and in the absence of *Hes7*, somites fuse (Bessho et al., 2001b). Interestingly, persistent activation of *HES7* also leads to somite fusion (Hirata et al., 2004). Another HES family member, *Hes6/HES6,* has been shown to regulate differentiation and fusion of myoblasts and its overexpression is predictive of poor prognosis in alveolar rhabdomyosarcoma (ARMS) (Gao et al., 2001, Malone et al., 2011, Wickramasinghe et al., 2013). These data suggest that HES genes have dual roles in mesodermal specification and myogenesis, but *HES3*, a neural transcription factor, has not been implicated in these processes.

Previously, we identified a role for *HES3* in fusion-positive rhabdomyosarcoma, a pediatric cancer that resembles immature skeletal muscle and is characterized by an inability to terminally differentiate (Parham and Ellison, 2006). We found that injecting the human *PAX3-FOXO1* fusion, the defining oncogene in a subset of alveolar rhabdomyosarcoma (Barr et al., 1993, Barr, 2011), into zebrafish embryos significantly upregulated *her3* mRNA expression. Further, *her3* overexpression was unique to and dependent on *PAX3-FOXO1*. Our finding is translatable to the human disease, as *HES3* is overexpressed in fusion-positive alveolar rhabdomyosarcoma patient tumors, and this overexpression is predictive of reduced overall survival (Kendall et al., 2018). This suggests that *HES3* has functional consequences when expressed in fusion-positive ARMS. Given that other HES genes are implicated in myogenic and tumorigenic processes, we sought to understand how *her3*/*HES3* could be contributing to this disease.

Here, we make a series of *her3* CRISPR/Cas9 null mutant alleles in zebrafish to investigate *her3's* role in developmental processes and probe how this could translate to its role during tumorigenesis. We show that loss of *her3* is not embryonic lethal and progeny exhibit the expected Mendelian ratios. Mutant *her3* is unable to bind a known target gene *neurog1*, resulting in an expansion of overall *neurog1* expression in *her3* mutants. In addition, *her3*

null mutation results in significant reduction of overall size in zebrafish embryos and lens degradation in a subset of fish as adults. Our RNA-seq analysis of differentially expressed genes of early zebrafish embryos suggests: 1) an enrichment of genes involved in the inhibition of matrix metalloproteinases; and 2) an enrichment for Sox10-regulated genes, a neural crest-specific transcription factor. These functions during neural development, stem cell maintenance, and extracellular matrix (ECM) homeostasis could be important for *her3/HES3*'s role as a cooperating gene in fusion-positive ARMS. Our new animal model is a powerful system to study these outstanding questions.

Materials and Methods

Zebrafish Humane Use and Husbandry

Zebrafish are housed in an AAALAC-accredited, USDA-registered, OLAW-assured facility in compliance with the Guide for the Care and Use of Laboratory Animals. All research procedures are approved by the IACUC at The Abigail Wexner Research Institute at Nationwide Children's Hospital according to IACUC protocol AR19–00172. Zebrafish are free of Pseudoloma neurophilia, Pleistophora hyphessobryconis, Pseudocapillaria tomentosa, Mycobacterium spp., Edwardsiella ictalurid, Ichthyophthirius multifilis, Flavobacterium columnare, and zebrafish picornavirus (ZfPV1) as determined by quarterly sentinel monitoring program. The fish were housed at a density of 8–12 fish per liter in mixed-sex groups in 0.8 L, 1.8 L, 2.8 L, or 6 L tanks on a recirculating system (Aquaneering, San Diego, CA) in 28ºC water (conductivity, 510 to 600 μS; pH, 7.3 to 7.7; hardness, 80 ppm; alkalinity, 80 ppm; dissolved oxygen, greater than 6 mg/L; ammonia, 0 ppm; nitrate, 0 to 0.5 ppm; and nitrite, 0 ppm) in a room with a 14:10-h light:dark cycle. System water was carbon-filtered municipal tap water, filtered through a 20-μm pleated particulate filter, and exposed to 40W UV light. The fish were fed twice daily with both a commercial pelleted diet and a live brine shrimp cultured in-house. WIK were used as the wildtype line and were obtained from the Zebrafish International Resource Center (ZIRC; https://zebrafish.org). *her3* mutant zebrafish will be made available upon request and will be deposited at ZIRC.

Cloning

pCS2+MCS-P2A-sfGFP was a gift from Jason Berman (Addgene plasmid # 74668; http://n2t.net/addgene:74668; RRID:Addgene_74668) (Prykhozhij et al., 2017). pCS2-TagRFPT.zf1 was a gift from Harold Burgess (Addgene plasmid # 61390; http://n2t.net/addgene:61390; RRID:Addgene_61390) (Horstick et al., 2015). RNA was collected from zebrafish embryos from either wildtype WIK or homozygous *her3*-null mutants using QIAGEN RNeasy Mini kit (74104, QIAGEN). Then, cDNA was synthesized using the RT2 HT First Strand Synthesis kit (330411, QIAGEN). PCR was done using the cDNA and primers against the *her3* coding sequence (Table S1), adding a PacI site on the 5' end and an AscI site on the 3' end. PCR products were cleaned up using the Monarch PCR Cleanup kit (T1030L, NEB). A double digest using PacI and AscI was done on the PCR products and the pcs2+MCS-P2A-sfGFP plasmid, and then cleaned up using the Monarch PCR Cleanup kit (T1030L, NEB). Digested PCR products were then ligated to the digested pcs2+MCS-P2A-sfGFP plasmid using T4 DNA ligase (M0202S, NEB) in a 3:1 insert:backbone ratio. Ligated

plasmids were transformed into DH5α cells (FEREC0111, Fisher Scientific). Colonies were picked and sequenced via Sanger sequencing by Eurofins Genomics to verify insert. Final plasmids were named pcs2+*her3*^{WT}-P2A-sfGFP, pcs2+*her3*^{nch1}-P2A-sfGFP, pcs2+*her3*^{nch2}-P2A-sfGFP, and pcs2+*her3*^{nch3}-P2A-sfGFP. Using this same strategy, a 3x FLAG-tag was cloned onto the 3' end of both WT and *her3*^{nch1} cDNA using primers specific to the 3' end of each *her3* cDNA (Table 1). These 3' FLAG-tagged products were then ligated into the pcs2+MCS-P2A-sfGFP plasmid.

Zebrafish Embryo Injections

Zebrafish were injected at either the 1-cell stage in the cell body for CRISPR/Cas9 injections, or the 1–4 cell stage in the yolk for RNA and morpholino injections. For CRISPR/Cas9 injections, embryos were injected with 36ng/μl crRNA and 67ng/μl of tracrRNA for one of three gRNAs against the *her3* locus (Table S1), 100 ng/μl Cas9 protein (IDT), 0.1% phenol red, and 0.3X Danieau's buffer. For RNA injections, embryos were injected with: 100 ng/μl RNA of either pcs2+*her3*^{WT}-P2A-sfGFP, pcs2+*her3*^{nch1}-P2A-sfGFP, pcs2+*her3*^{nch2}-P2A-sfGFP, or pcs2+*her3*^{nch3}-P2A-sfGFP; 50ng/μl RNA of pcs2-tagRFPT.zf1; 0.1% phenol red; and 0.3X Danieau's buffer. Separately, embryos were injected with: pcs2+*her3*^{WT}-3xFLAG-P2A-sfGFP, or pcs2+*her3*^{nch1}-3xFLAG-P2A-sfGFP; 0.1% phenol red; and 0.3X Danieau's buffer. For morpholino injections, embryos were injected with: 200μM of either *her3*-MO1 or mm-MO (Table S1); 0.1% phenol red; and 0.3X Danieau's buffer. Morpholinos were custom ordered from GeneTools.

High Resolution Melt Analysis

CRISPR mutant alleles were identified using High Resolution Melt Analysis (HRMA). Either embryos or fin clips were used to generate genomic DNA for HRMA. A minimum of three wildtype (WIK) samples were included with each HRMA as the reference group. Briefly, individual 24hpf embryos or adult fin clips were incubated in 10 mM Tris-HCl pH 8.3, 50mM KCl, 0.3% Triton X-100, and 0.3% NP40 for 10 minutes at 98°C, then cooled on ice for 10 minutes. Then, 1/10th volume of 10 mg/ml Proteinase K (BP1700, Fisher Scientific) was added and samples were incubated overnight at 55°C, heated to 98°C for 10 minutes to heat-inactivate proteinase K, and cooled to between 4°C and 12°C. For HRMA, 200ng of genomic DNA, 9μl of Precision Melt Mix (1725112, Bio-Rad), 0.5μl of each of forward and reverse primers (Table S1), and water up to 20μl was added to a 384-well PCR plate. The plate was then run on a Bio-Rad CFX384 Real Time PCR Detection System using the following program: 95°C for 3 minutes; (95°C for 15 seconds, 60°C for 20 seconds, 70°C for 20 seconds) x 45 cycles; 65°C for 30 seconds; melt 65°C-95°C, 0.2°C/step hold 5 seconds; 95°C for 15 seconds. The real-time data file was then opened on Bio-Rad Maestro software to generate a .PCRD file. The .PCRD file was then opened on Bio-Rad Precision Melt Analysis software. Known wildtype WIK samples were used as the reference group. Samples with a Difference RFU between 0.1 and −0.1 were excluded.

Western Blotting

Western blotting was done on 6hpf zebrafish embryos. Briefly, separate pools of WIK, *her3*^{nch1}, *her3*$^{nch1/nch2}$, and *her3*^{nch3} embryos were dechorionated at 6hpf using pronase, deyolked (55 mM NaCl, 1.8 mM KCl, 1.25 mM $NaHCO_3$), and washed with 0.5X

Danieau's buffer (29 mM NaCl, 0.35 mM KCl, 0.2 mM $MgSO_4 \cdot 4H_2O$, 0.3 mM $Ca(NO_3)_2 \cdot 4H_2O$, 2.5 mM HEPES). Embryos were then snap frozen with dry ice and stored at −80°C. Embryo lysates were created by adding 2 μl/embryo of 2x Laemmli Buffer (1610737, BIO-RAD) and heating at 95°C for 5 minutes. The lysates were then spun down at max speed for 1 minute before loading 20μl of each sample into a 4–15% gradient mini-PROTEAN TGX gel (4561084, BIO-RAD). Samples were run at 150V, then transferred to a 0.2μm PVDF membrane (1620177, BIO-RAD) at 100V for one hour. The membrane was blocked for one hour in Casein block solution (PI37528, Fisher Scientific) with 0.05% Tween-20, then incubated overnight at 4˚C with primary antibody: mouse anti-Tubulin at 1:1000 concentration (3873S, Cell Signaling) and rabbit anti-HES3 at 1:500 concentration (PA567801, Thermo Scientific) in new Casein block solution with 0.05% Tween-20. Blots were then washed with 1x PBS with 0.05% Tween-20 and incubated for 1 hour with secondary antibody: goat HRP-anti-mouse at 1:10,000 concentration (1706516, BIO-RAD) and goat HRP-anti-rabbit at 1:10,000 concentration (1721019, BIO-RAD). Blots were then washed again with 1x PBS with 0.05% Tween-20, then imaged on a C-DiGit Chemiluminescent LI-COR imager (103375–240, VWR). Tubulin blots were imaged with SuperSignal West Pico PLUS Chemiluminescent Substrate (PI34577, Fisher Scientific) and Her3 blots were imaged with SuperSignal West Atto Ultimate Sensitivity Chemiluminescent Substrate (PIA38554, Fisher Scientific).

Real Time Quantitative PCR

Real time qPCR was done on both 24hpf and 72hpf zebrafish embryos. Briefly, 3 pools of 10 embryos from each of WIK, *her3*^{nch1}, *her3*^{nch2}, and *her3*^{nch3} at both 24hpf and 72hpf were collected. Additionally, 3 pools of 10 embryos each of WIK embryos injected with either *her3*-MO1 or mm-MO (Table S1) at 24hpf were collected. RNA was isolated from each of the pools of embryos using the QIAGEN RNeasy Mini kit (74104, QIAGEN) including an on-column DNAse digestion. The RT2 HT First Strand Synthesis kit (330411, QIAGEN) was used to synthesize cDNA using 160ng of RNA per sample. cDNA was diluted to 80μl with nuclease-free water. A mastermix containing 5μl SYBR Green 2x (1725122, Bio-Rad) and 0.5μl of each 10mM forward and reverse primer, per sample, was combined with 4μl of cDNA in a 384-well PCR plate. The plate was run on a CFX384 Real Time PCR Detection System using the following program: 95°C for 2 minutes; (95°C for 15 seconds, 60°C for 1 minute, Plate Read) x 40 cycles; 65°C for 30 seconds; (65°C, 0.5°C/step, Plate Read) x 60 cycles. The real time data file was then opened on Bio-Rad CFX Maestro software to generate a .PCRD file. The software was then used to determine differential gene expression using the ΔΔCT method. Housekeeping genes used: *rpl13a* and *actinb1* (Table S1). Genes queried: *her3* (Table S1).

Adult Zebrafish Tissue Collection and Staining

Adult zebrafish were euthanized in a 2mg/mL Tricaine-S solution. They were then fixed for 24 hours at room temperature in 4% PFA, then decalcified in 0.5M EDTA pH 7.8 for 5 days at room temperature. Zebrafish were then mounted in paraffin blocks for microtome sectioning. Sections were taken in 8μm intervals. De-paraffinized slides were then stained with Hematoxylin and Eosin as previously described (Kendall and Amatruda, 2016).

RNAscope and Nuclear Staining

For RNAscope, 11hpf or 24hpf zebrafish embryos from both WIK and *her3*^{nch1} homozygous in-crosses were collected. The RNAscope Assay on Whole Zebrafish Embryos as well as the RNAscope Multiplex Fluorescent v2 (323100, Advanced Cell Diagnostics) manuals were followed. The dre-*her3* probe (895001-C2, Advanced Cell Diagnostics) and dre-*neurog1* probes (505081-C2) were used with DAPI provided in the Multiplex Fluorescent kit. Opal 520 (NC1601877, Fisher Scientific) and Opal 570 (NC1601877, Fisher Scientific) were used. Embryos were imaged on both a Zeiss LSM800 inverted confocal microscope with a 20x objective and a Leica M205FA fluorescent stereoscope with a 2x objective. Image analysis and quantification of area and integrated density were performed in ImageJ version 1.53h.

ChIP-qPCR

ChIP protocol was adapted for zebrafish cells from (Sunkel et al., 2021). WIK in-cross zebrafish embryos were injected with 50ng/μL of *her3*^{WT} or *her3*^{nch1} mRNA at the single-cell stage. Embryos were incubated in E3 at 32.0ºC for 5 hours and 15 minutes. Following incubation embryos were dechorionated with pronase, deyolked (55mM NaCl, 1.8mM KCl, 1.25mM $NaHCO_3$), and washed with 0.5X Danieau's buffer (29mM NaCl, 0.35mM KCl, 0.2mM $MgSO_4 \cdot 4H_2O$, 0.3mM $Ca(NO_3)_2 \cdot 4H_2O$, 2.5mM HEPES). Embryos were pipetted with P200 to obtain single cell suspension in dPBS. Cells were fixed at room temperature in 1% formaldehyde for 10 minutes and quenched with a final concentration of 125mM glycine on ice for 5 minutes. Cells were snap-frozen with dry ice and stored at −80ºC until sonication. RH30 cells were cultured in T175 flasks and lifted with TrypLE Express before fixation following similar method as described above. Rh30 cells (CRL-2061, ATCC) are serving as carrier chromatin. 1 million injected zebrafish and 1 million Rh30 cells were thawed, combined, and suspended in 800μL of TE buffer, pH 8.0 with protease inhibitors. Samples were sonicated with an Active Motif EpiShear probe sonicator at 30% amplitude with a 30 second on/off cycle for 10 minutes while on a cooling block in polystyrene micro centrifuge tubes. Following sonication, 5μL were taken for reverse crosslinking in 20μL TE, 1μL 10% SDS, and 1μL 18.5mg/mL Proteinase K with 65ºC overnight incubation. DNA was purified Qiagen MinElute PCR Purification kit, eluted in 36μL EB, and DNA fragmentation was checked using E-Gel 2% EX agarose gel system. These samples serve as input controls and were stored at 4ºC until qPCR evaluation. 770μL of the remaining chromatin was taken and had buffer adjusted to 1% Triton X-100, 0.1% SDS, 0.1% sodium deoxycholate, and 200mM NaCl. To remove cellular debris, chromatin supernatant was transferred to a clean microcentrifuge tube following 5 minutes incubation on ice and 10 minute centrifugation at 13,000rpm at 4ºC. Chromatin was incubated with 4μg of FLAG antibody (F1804, Sigma-Aldrich) for 2 hour overhead rotation at 4ºC. Incubation continued overnight with addition of 40μL of Protein G Dynabeads (10–003-D, Fisher Scientific). Non-specific DNA was removed by stringency washes. Samples were washed twice in TE with 0.1% SDS, 0.1% sodium deoxycholate, and 1% Triton X-100 , twice in TE with 1% Triton X-100, 0.1% SDS, 0.1% sodium deoxycholate, and 200mM NaCl, twice in TE with 250 mM LiCl, 0.5% NP-40, 0.5% sodium deoxycholate, and once with TE. Finally, chromatin underwent reverse crosslinking at 65ºC overnight with 100μL TE, 2.5μL 10% SDS, and 5μL 18.5mg/mL Proteinase K. DNA was purified with QIAGEN MinElute PCR

Purification kit, and eluted in 36μL EB buffer. IP and input DNA were diluted 1:2 with H_2O and run in triplicate with *neurog1* primers surrounding a known Her3 binding site (Table S1) (Hans et al., 2004) and a negative control, to which Her3 was not predicted to bind (71036, Active Motif).

RNA-seq

RNA-seq was performed on both 24hpf and 72hpf embryos. Three pools of 20 embryos each of WIK, *her3*^{nch1}, WIK injected with *her3*-MO1, and WIK injected with mm-MO at 24hpf, and of WIK and *her3*^{nch1} at 72hpf, were staged and then collected. RNA was immediately isolated using the QIAGEN RNeasy Mini kit with on-column DNAase digestion (74104, QIAGEN). RNA integrity and sample QC was determined by the Nationwide Children's Hospital Institute for Genomic Medicine (IGM) using an Agilent Bioanalyzer 2100. WIK 24hpf samples were spiked with 2μl of 1:100 diluted ERCC spike-in mix 1 (4456740, Thermofisher Scientific) while all other samples were spiked with 2μl of 1:100 diluted ERCC spike-in mix 2 (4456740). Sequencing libraries were generated using the NEBNext Ultra II Directional RNA Library Prep Kit for Illumina (E7760, New England Biolabs). A polyA enrichment step (E7490, New England Biolabs) was used to enrich for polyadenylated RNAs. RNA samples were run on a NovaSeq SP with 150bp paired-end reads and a total of 43–51 million reads generated output per sample (Table S2, Figure S6).

RNA-seq Analysis

All RNA-seq analyses were performed on the Nationwide Children's Hospital high-performance cluster. The cluster is running CentOS 8.1 with a slurm job manager. All code used in analyzing the RNA-seq data is freely available online (https://github.com/MVesuviusC/kentRNAseq1). We used FASTQC (v0.11.9) to evaluate sequence data quality. We created a dual reference containing both the zebrafish genome (danRer11) as well as the ERCC spike-in reference sequences to use for alignment with HiSat2 (v 2.2.1) (Kim et al., 2019). We allowed for only a single alignment per read (−k 1), and then removed PCR duplicates and removed any improperly paired reads with SAMtools (v1.10) (Li et al., 2009). To count the number of reads per gene, we employed the featureCounts program from Subread (v2.0.2) package (Liao et al., 2014). We performed statistical analysis of differential expression using the EdgeR R package (v 3.34.0) (Robinson et al., 2010). To call differentially expressed genes we used an FDR cutoff of less than or equal to 0.1 and a fold-change cutoff of either greater than or equal to 1.5 or less than or equal to −1.5. For motif analysis, we used HOMER (v4.11.1) (Heinz et al., 2010). Plotting and data manipulation were primarily done using the tidyverse suite of R packages (Wickham et al., 2019).

Statistics

GraphPad Prism 9 and R were used for all statistical analysis. A chi-square test was used to determine if observed zebrafish clutches were significantly different from expected Mendelian ratios (Figure S3). A one-way Brown-Forsythe and Welch ANOVA with a Dunnett T3 test was used to determine significance of GFP expression (Figure 2C). A one-way ANOVA with Dunnett test was used to determine significance of *her3* expression (Figure 3A-B), 24hpf embryo length (Figure 5E), and adult length (Figure S4E). A two-

tailed Welch's t-test was done to determine significance of RNAscope *her3* expression (Figure 3F), RNAscope scores (Figure 4C-D), *neurog1* and *her3* expression fold change (Figure 4E), fold enrichment binding (Figure 4F), and 72hpf embryo length (Figure 5H). All sample sizes are included in figure legends.

Data and Code Availability

All data is freely available through the NCBI GEO repository (GSE196814) and all code is available on GitHub (https://github.com/MVesuviusC/kentRNAseq1).

Results

Generating and validating *her3* null mutations in zebrafish.

To generate *her3* frameshift mutations in zebrafish, we used a CRISPR/Cas9 method adapted from the Talbot and Amacher protocol (Talbot and Amacher, 2014). Wildtype WIK zebrafish embryos were injected at the 1–2 cell stage in the cytoplasm with a *her3* gRNA and Cas9 protein (Figure 1A). The *her3* gRNA resulted in multiple potential mutations in P0 crispants, as determined by High Resolution Melt Analysis (HRMA) (Figure S1). Injected embryos were allowed to develop to sexual maturity (~ 3 months), and then were screened as potential founders by outcrossing to wildtype WIK and analyzing F1 offspring using HRMA. This strategy identified six potential founders from which one founder with the most diverse mutations was chosen to generate an F1 population (Figure S2). HRMA screening of the adult F1 heterozygous offspring revealed three potential mutations (Figure 1B). To determine the exact mutation, the region surrounding the gRNA binding site was A-tail cloned, sequenced, and analyzed via translation prediction (Figure 1C). The first mutation identified was a 4bp deletion, resulting in a frameshift after the 37th amino acid, an altered 38th amino acid, and a premature stop codon. The second mutation identified was a 7bp deletion resulting in a frameshift after the 38th amino acid, 25 additional altered amino acids, and a premature stop codon. The third mutation identified was a 20bp insertion resulting in a frameshift after the 42nd amino acid, 30 additional altered amino acids, and a premature stop codon. These are each referred throughout the text as: *her0*^{nch1}, *her3*^{nch2}, and *her3*^{nch3}, respectively. Mutation sites and qPCR binding sites are shown in Figure S5. Each of these three mutations was a potential knockout, with the frameshift occurring in the middle of the DNA binding domain (Figure 1C).

We verified *her3* mutants were indeed knockouts using a variety of approaches. First, we utilized an adapted reporter assay (Prykhozhij et al, 2017). Zebrafish *her3* cDNA was amplified from either wildtype WIK or the three *her3* homozygous mutant lines and cloned into the pCS2-MCS-P2A-sfGFP vector. Four separate rounds of injections were done, each with RNA from one of the constructs (*her3*^{WT}, *her3*^{nch1}, *her3*^{nch2}, or *her3*^{nch3} mutant alleles), as well as RNA from pCS2+TagRFPT as an injection control. The RNAs were co-injected into the yolk of wildtype WIK embryos at the 1–4 cell stage (Figure 2A). At 24 hours post-fertilization (hpf), individual embryos were then imaged for GFP expression (*her3* construct) and RFP expression (control construct). Each of the three lines tested - *her3*^{nch1}, *her3*^{nch2}, and *her3*^{nch3} - exhibited a significant decrease in GFP/RFP fluorescence ratio compared to the wildtype *her3* RNA (Figures 2B-C). We also identified a human

HES3 antibody that cross-reacted with zebrafish Her3. Additional testing by western blot with a HES3/Her3 antibody showed complete lack of full-length Her3 protein for *her3*^{nch1} and *her3*^{nch3} in homozygous embryos, and *her3*^{nch1}/*her3*^{nch2} as a compound heterozygote (Figure 2D). These data indicate the mutant zebrafish are indeed knockouts for the full-length Her3 protein.

her3 knockout fish are viable as adults.

We generated F2 adult homozygous fish from the three *her3* knockout lines. The progeny of heterozygote in-crosses had normal survival as embryos, juveniles, and adults (Figure S3). After tail clipping and performing a HRMA for zygosity, we did not observe a significant deviation from the expected Mendelian ratios for all three potential mutants as determined by chi-square test (Figure S3). These data indicate that *her3* knockout is not lethal, which is similar to the *Hes3* mouse knockout that has been described (Hirata et al, 2001). Interestingly, 20% of adult *her3*^{nch1} fish have abnormal eye development (Figure S4A-D). These fish with abnormal eye development are significantly smaller than wildtype fish as adults, but show no other gross morphological changes (Figure S4E-H). Further, homozygous *her3* mutant fish are viable and are capable of producing offspring that develop into adulthood.

her3 knockout embryos exhibit de-regulation of *her3* and a *her3* target gene, *neurog1*

A previous study of Her3 activity in zebrafish showed that Her3 directly regulates its own expression by binding DNA and acting as a transcriptional repressor. Knocking down *her3* via morpholino (MO) results in an increase in *her3* mRNA expression (Hans et al, 2004). Similarly, we found that at 24hpf, *her3* knockout also results in an increase in *her3* mRNA expression in all three *her3* mutant alleles. This expression phenocopies a *her3* morpholino knockdown (Figures 3A and 3B). By 24hpf, *her3* expression is spatially restricted to portions of the brain and tail as determined by fluorescent in-situ hybridization using a custom *her3* RNAscope probe, and is consistent with previous reports (Thisse and Thisse, 2005) (Figures 3C-E). In the tail, we find an expansion of *her3* mRNA in knockout fish as compared to wildtype controls (Figure 3D-F), suggesting inappropriate spatial distribution.

To further investigate early loss of Her3 activity on direct targets, we evaluated regulation and binding of *neurog1*. Previous studies found that *her3* knockdown resulted in increased, diffuse expression of *neurog1* in zebrafish development starting at 11hpf (Hans et al., 2004). At 11hpf, we found *her3* knockout resulted in increased expression of *neurog1* by RNAscope (Figure 4A-D). Additionally, qRT-PCR showed increased expression of both *her3* and *neurog1* at this timepoint (Figure 4E). We also performed a functional assessment of *her3*^{wt} and *her3*^{nch1} mutant binding at a known site in the *neurog1* promoter. To do this, we injected FLAG-tagged *her3* RNA from *her3*^{WT} or *her3*^{nch1} zebrafish into wildtype embryos. We performed a FLAG ChIP and qRT-PCR around a known Her3 binding site in the *neurog1* promoter region. Wildtype Her3 was significantly enriched at the *neurog1* promoter, whereas *her3*^{nch1} mutant binding was not observed at this site (Figure 4F). These data are functional validation that the *her3*^{nch1} mutant is unable to bind *neurog1* promoter DNA and act as a transcriptional repressor.

her3 null mutants have reduced overall size

All *her3* homozygous mutants appeared smaller than stage-matched wildtype embryos by 24hpf. To quantify this effect, we imaged 24hpf embryos and measured the standard length. This revealed that *her3* null mutants were significantly smaller (Figures 5A-E). However, by 72hpf, the standard length of *her3* null mutant embryos is indistinguishable from wildtypes, suggesting later compensatory mechanisms can rescue this early growth defect (Figures 5F-H). We decided to move forward with only the *her3*^{nch1} line because all three mutant lines were functionally similar based on the *her3* qPCR assay and standard length (Figures 3A, 5E) and because the mutation in *her3*^{nch1} produces the shortest protein product (Figure S5).

her3 null mutation alters the zebrafish embryo transcriptome

To more broadly investigate the impact of *her3* loss on zebrafish development, we performed RNA-seq on *her3*^{nch1} mutants and wildtype fish at 24hpf and 72hpf. We chose these timepoints because previously we found that *her3* was up-regulated in the context of *PAX3-FOXO1* fusion-oncogene expression in 24hpf zebrafish embryos. Further, concurrent overexpression of *HES3* and *PAX3-FOXO1* increased the number of *PAX3-FOXO1* positive cells persisting between 24hpf and 72hpf in zebrafish embryos (Kendall et al., 2018). We also injected wildtype zebrafish with *her3*-MO and mm-MO and harvested injected embryos at 24hpf for comparison to the *her3* mutant. A schematic of the timepoints and groups used is in Figure 6A. Read counts are presented in Table S2 and read alignment in Figure S6A-B. Pairwise correlations were also plotted (Figure S7). Normalized read counts for *her3* expression were graphed (Figure S8), validating the previous qRT-PCR data (Figure 3A-B). For all samples, a principal component analysis (PCA) was done in which the 24hpf samples clustered together separately from the 72hpf samples, indicating that the biggest difference for demarcating groups is reflective of developmental stage (Figure 6B). Further, the morpholino samples clustered together but separately from other 24hpf samples, suggesting there are inherent differences in uninjected and injected zebrafish (data not shown).

A separate PCA analysis in Figures 6C-D de-coupled developmental changes between 24 to 72hpf from the effects of the *her3* mutation. We therefore re-analyzed and re-clustered the 24 and 72hpf data presented in Figures 6C-D to appreciate the variation between those samples in the absence of the extreme variance we see across timepoints. A PCA of each timepoint independently showed that *her3*^{nch1} clusters separately from WIK (Figures 6C-D). All differentially expressed genes (logFC 1.5) were plotted using hierarchical clustering, indicating that WIK and *her3*^{nch1} zebrafish largely have the same expression patterns within the same timepoint (Figure 6E). We then focused on individual differentially expressed genes at 24hpf or 72hpf in *her3* mutants as compared to WIK visualized with volcano plots (Figures 6F-G). This highlights that the magnitude of change was amplified by 72hpf, and of interest were modulated genes such as *pctp*, which is involved in digestive tract and liver development (Zhai et al., 2017) and was significantly downregulated at 72hpf, and *csrp1b,* a cysteine-rich LIM-domain protein involved in myogenesis and fibroblast development (Iuchi and Kuldell, 2005, Bach, 2000), which was significantly downregulated at 24hpf. We found no transcriptional upregulation or evidence of compensation by other *her* family genes.

Figure 6H is a summary of the pairwise comparisons of up- and downregulated genes for each group, of which we focused on the *her3*-WIK 24hpf and 72hpf comparisons in Figure 7.

We then assessed differentially expressed genes that were shared between the 24hpf and 72hpf timepoints for *her3* mutants as compared to wildtype embryos. These genes could suggest embryonic programs that are most impacted by the *her3* mutation or that inappropriately persist. A comparative analysis between the 24hpf and 72hpf timepoints was performed, first looking at which differentially expressed genes are shared between the two timepoints. This analysis indicates a total of 70 genes upregulated at both 24hpf and 72hpf in *her3*^{nch1}, and 134 genes that are shared and downregulated (Figures 7A-B). Shown are the annotated differentially expressed genes that are shared and unique for each of these timepoints. One gene of interest was *grinab*, downregulated at both 24hpf and 72hpf, which helps regulate apoptosis of the nervous system during development, further highlighting the mis-regulation of developmental processes in the *her3* null mutant (Rojas-Rivera et al., 2012). A full list of the shared up- and downregulated genes is in Table S3. Further, a HOMER motif analysis was conducted on promoter regions of differentially expressed genes to identify transcriptional regulators outside of *her3* that are being impacted in the mutants. A single known motif was significantly enriched, Irf1, from the 72hpf samples with an adjusted p-value of 0.0304. However, 26 *de novo* motifs were identified in promoters of differentially expressed genes as significantly enriched in the 24hpf samples and 29 in the 72hpf samples. At 24hpf, three different *de novo* motifs for forkhead family members were identified (Foxp3, Foxq1, and Foxh1) while Foxo1 was enriched in the 72hpf samples. The binding motif of a single transcription factor was significantly enriched between 24hpf and 72hpf: the motif for Sox10 (Figure 7C-D). This is perhaps not too surprising as SOX10 is known for its role in neural crest development, but intriguingly, it is also highly expressed with functional consequences in multiple cancers such as glioma, glioblastoma, and melanoma (Pingault et al., 2022). A full list of enriched motifs is presented in Table S4.

Finally, an Ingenuity Pathway Analysis (IPA) was performed on differentially expressed genes between the *her3* mutant and wildtype embryos at both 24 hours and 72 hours post fertilization (Figure 7E), a full list of which can be seen in Figure S9. This analysis identified genes enriched within shared pathways at both timepoints, and uniquely at the 24hpf or 72hpf timepoint. Notably, the 24hpf timepoint had enrichment for pathways involved in neuroinflammation and neural development, suggestive of Her3's normal role during this time period, whereas the 72hpf timepoint was enriched for Spink1 mediated carcinogenesis. The most enriched and shared pathway between both 24hpf and 72hpf timepoints was an inhibition of matrix metallopeptidases, which is consistent with our previous data indicating that *HES3* overexpression in Rh30 *PAX3-FOXO1* rhabdomyosarcoma patient cancer cells increases *MMP3/9* expression (Kendall et al., 2018). These data correlated between the fish and human, indicating that the modulation of this pathway could have a role in ARMS pathogenesis.

Discussion

Here, we created a zebrafish *her3* null mutant line to investigate Her3*'s* role in development and how these processes are potentially being co-opted in alveolar rhabdomyosarcoma. We generated a series of zebrafish *her3* mutant alleles using CRISPR/Cas9 and found that these mutations were not embryonic lethal and displayed the expected Mendelian ratios. We demonstrated that these lines are functional nulls by showing early deregulation of *neurog1* expression and lack of binding by the *her3*^{nch1} mutant to the *neurog1* promoter. We showed that the *her3* null mutant zebrafish embryos are significantly smaller than their wildtype counterparts at 24 hours post fertilization, and that as a transcriptional repressor, removing *her3* negatively impacts appropriately controlled development. Our RNA-seq data showed that certain genes and pathways were identified as Her3-regulated across multiple timepoints. This includes an enrichment for Sox10 binding motifs and regulation of genes involved in matrix metalloproteinase pathways. Taken together, these data further implicate *her3*/*HES3* in fusion-positive rhabdomyosarcoma pathogenesis, with a potential role in suppressing differentiation in these immature skeletal muscle-like tumors.

Previously, zebrafish *her3* has been investigated in early developmental stages to understand its role in transcriptional repression. One study found that *her3* is a transcriptional repressor of *neurog1* in early development (through the 16-somite stage) and that *her3* itself is repressed by Notch signaling (Hans et al., 2004). A more recent study identified *her3* as a target of *pou5f1*, an ortholog of *OCT4*, and refined *her3's* maximum expression to between 7–8hpf (Onichtchouk et al., 2010). While we saw no significant change in *neurog1* mRNA levels at 24hpf in the *her3* null mutant fish, earlier regulation of *neurog1* was significantly impacted by *her3* null mutation. These data include loss of Her3 binding in the *neurog1* promoter region and an expansion in area of *neurog1* expression (Figure 4).

In this study, our data provides valuable insight to the longer-term effects of the loss of a developmental transcription factor that normally possesses a finite expression window. While the number of differentially expressed genes may be few at these later timepoints (Figure 6H), the effects appear to be far reaching. In the *her3*^{nch1} mutants, reduced gene expression of *pctp, csrp1b,* and *grinab,* all genes involved in organ development, could explain the reduced size seen in mutant embryos and eye defects in a subset of adults. Another possibility is that Her3 has an additional function other than transcriptional repression. Recently, the bHLH transcription factor MYOD was found to be a genome organizer, helping to define the 3D structure of chromatin during myogenesis with little impact on gene expression levels (Wang et al., 2022). It is possible that the bHLH Her3/HES3 is acting in a similar manner during development, organizing chromatin in a specific 3D structure throughout the whole embryo at early timepoints, and in neural tissue later in development (Thisse and Thisse, 2005). This is a direction that we plan on investigating further.

Mouse *Hes3*, the ortholog to zebrafish *her3*, is involved in the regulation of neural development and poising neural stem cells to differentiate or divide (Poser et al., 2013). Additionally, higher *Hes3* expression has been linked to increased cellular proliferation (Masjkur et al., 2014, Park et al., 2013, Poser et al., 2014). It is therefore not surprising

that human *HES3* is overexpressed in multiple cancer types with functional consequences. *HES3* was found to enhance the malignant phenotype in non-small cell lung cancer (NSCLC) and facilitated poor differentiation, increased metastasis, and worse patient prognosis. Further, *HES3* expression in NSCLC tissue upregulated cyclin D1, cyclin D3, and MMP7 (Fang et al., 2019). Our previous work found that *HES3* is a cooperating gene in *PAX3-FOXO1* fusion-driven alveolar rhabdomyosarcoma. Overexpression of *HES3* predicted reduced overall survival in patients; however, the mechanism for *HES3* and *PAX3-FOXO1* cooperation in fusion-positive rhabdomyosarcoma is unclear (Kendall et al., 2018). The similarities in *HES3* expression in NSCLC and alveolar rhabdomyosarcoma are suggestive. While cyclins are not differentially regulated in our zebrafish *her3* null mutant, *mmp9* is significantly downregulated, and the inhibition of the matrix metalloproteinase pathway is associated with *her3* mutant transcriptional signatures (Figure 7D). Additionally, our previous work showed that *HES3* overexpression in Rh30 PAX3-FOXO1 rhabdomyosarcoma patient cells upregulated *MMP3/9* expression (Kendall et al., 2018). This regulation of the matrix metalloproteinase pathway is indicative of a possible mechanism of cooperation in more aggressive cancer, as MMP3/9 facilitate metastasis (Nagase et al., 2006).

We also found Sox10 binding motifs to be enriched among the differentially expressed genes in the *her3* null mutant, which is suggestive of how Her3/HES3 may be functioning in these cancers (Figure 7D). A recent study in *Xenopus* found that overexpression of *hes3* resulted in an increase in *sox10* expression, which caused the neural crest progenitors to maintain an undifferentiated state (Hong and Saint-Jeannet, 2018). In addition to Sox10 motifs, several other motifs were identified that further links *her3* to cancer (Figure 7D). HIC1 and TWIST1 have been implicated in breast cancer (Wang et al., 2018, Martin et al., 2005). OLIG2 is highly expressed in gliomas and ARMS (Ligon et al., 2004, Raghavan et al., 2019). SIX1 has been shown to regulate cancer stem cell characteristics and to maintain the undifferentiated state in rhabdomyosarcoma (Kingsbury et al., 2019, Hsu et al., 2022). The enrichment of DNA binding motifs for these cancer-related genes is indicative of the strong link *her3* has to cancer contexts.

Overall, our new *her3* zebrafish null mutants are a powerful model with diverse utility to study development, cancer, and the consequences of their interface. Given that the mechanism of action of *HES3* in fusion-positive rhabdomyosarcoma is unclear, we plan to use this model to study how the *PAX3-FOXO1* fusion-oncogene functions with and without *her3/HES3*. Specifically, we will use this model as a baseline for both rescue by either zebrafish Her3 or human HES3, as well as overexpression with human HES3 in conjunction with human PAX3-FOXO1. By complementing these studies with the analysis of patient tumors and cell culture models, we anticipate that this model will help further elucidate how Her3/HES3 is acting in both development and cancer, which are intrinsically linked.

Supplementary Material

Refer to Web version on PubMed Central for supplementary material.

Acknowledgements

We thank Dr. Raphael Malbrue, Logan Fehrenbach, Adewole Adekanye, and the other Animal Resources Core Zebrafish Facility team members for exceptional care and collaboration in maintaining our zebrafish. We thank Emma Harrison and Amanda Jay for their technical support. We thank Dr. Stephen Lessnick for helpful discussion. We thank the Institute for Genomic Medicine, the NCH Morphology Core, and the NCH High Performance Computing group for providing services to support this study.

Funding Sources

This work was supported by NIH/NCI R01 grant R01CA272872, an Alex's Lemonade Stand Foundation "A" Award, a V Foundation for Cancer Research V Scholar Grant, and Startup Funds from The Abigail Wexner Research Institute at Nationwide Children's Hospital to G.C.K. M.K. is supported by a T32CA269052 Training Program in Basic and Translational Pediatric Oncology Research postdoctoral fellowship . D.C. is supported by a Graduate Enrichment Fellowship from The Ohio State University. The Institute for Genomic Medicine is funded by the Nationwide Foundation Pediatric Innovation Fund and the Ohio State University Comprehensive Cancer Center grant P30 CA016058. The funders had no role in study design, data collection and analysis, decision to publish, or preparation of the manuscript. Further, the content is solely the responsibility of the authors and does not necessarily represent the official views of the National Institutes of Health.

References

Androutsellis-Theotokis A, Leker RR, Soldner F, Hoeppner DJ, Ravin R, Poser SW, Rueger MA, Bae SK, Kittappa R & Mckay RD 2006. Notch signalling regulates stem cell numbers in vitro and in vivo. Nature, 442, 823–6. [PubMed: 16799564]

Androutsellis-Theotokis A, Rueger MA, Park DM, Mkhikian H, Korb E, Poser SW, Walbridge S, Munasinghe J, Koretsky AP, Lonser RR & Mckay RD 2009. Targeting neural precursors in the adult brain rescues injured dopamine neurons. Proc Natl Acad Sci U S A, 106, 13570–5. [PubMed: 19628689]

Artavanis-Tsakonas S, Rand MD & Lake RJ 1999. Notch signaling: cell fate control and signal integration in development. Science, 284, 770–6. [PubMed: 10221902]

Bach I 2000. The LIM domain: regulation by association. Mech Dev, 91, 5–17. [PubMed: 10704826]

Bae YK, Shimizu T & Hibi M 2005. Patterning of proneuronal and inter-proneuronal domains by hairy- and enhancer of split-related genes in zebrafish neuroectoderm. Development, 132, 1375–85. [PubMed: 15716337]

Barr FG 2011. Soft tissue tumors: Alveolar rhabdomyosarcoma. Atlas of Genetics and Cytogenetics in Oncology and Haematology

Barr FG, Galili N, Holick J, Biegel JA, Rovera G & Emanuel BS 1993. Rearrangement of the PAX3 paired box gene in the paediatric solid tumour alveolar rhabdomyosarcoma. Nat Genet, 3, 113–7. [PubMed: 8098985]

Bessho Y, Miyoshi G, Sakata R & Kageyama R 2001a. Hes7: a bHLH-type repressor gene regulated by Notch and expressed in the presomitic mesoderm. Genes Cells, 6, 175–85. [PubMed: 11260262]

Bessho Y, Sakata R, Komatsu S, Shiota K, Yamada S & Kageyama R 2001b. Dynamic expression and essential functions of Hes7 in somite segmentation. Genes Dev, 15, 2642–7. [PubMed: 11641270]

Davis RL & Turner DL 2001. Vertebrate hairy and Enhancer of split related proteins: transcriptional repressors regulating cellular differentiation and embryonic patterning. Oncogene, 20, 8342–57. [PubMed: 11840327]

Dubrulle J & Pourquie O 2004. Coupling segmentation to axis formation. Development, 131, 5783–93. [PubMed: 15539483]

Dunwoodie SL, Clements M, Sparrow DB, Sa X, Conlon RA & Beddington RS 2002. Axial skeletal defects caused by mutation in the spondylocostal dysplasia/pudgy gene Dll3 are associated with disruption of the segmentation clock within the presomitic mesoderm. Development, 129, 1795–806. [PubMed: 11923214]

El Yakoubi W, Borday C, Hamdache J, Parain K, Tran HT, Vleminckx K, Perron M & Locker M 2012. Hes4 controls proliferative properties of neural stem cells during retinal ontogenesis. Stem Cells, 30, 2784–95. [PubMed: 22969013]

Fang C, Jiang B, Shi X & Fan C 2019. Hes3 Enhances the Malignant Phenotype of Lung Cancer through Upregulating Cyclin D1, Cyclin D3 and MMP7 Expression. Int J Med Sci, 16, 470–476. [PubMed: 30911281]

Gajewski M & Voolstra C 2002. Comparative analysis of somitogenesis related genes of the hairy/Enhancer of split class in Fugu and zebrafish. BMC Genomics, 3, 21. [PubMed: 12160468]

Gao X, Chandra T, Gratton MO, Quelo I, Prud'homme J, Stifani S & St-Arnaud R 2001. HES6 acts as a transcriptional repressor in myoblasts and can induce the myogenic differentiation program. J Cell Biol, 154, 1161–71. [PubMed: 11551980]

Hans S, Scheer N, Riedl I, V Weizsacker E, Blader P & Campos-Ortega JA 2004. her3, a zebrafish member of the hairy-E(spl) family, is repressed by Notch signalling. Development, 131, 2957–69. [PubMed: 15169758]

Hatakeyama J, Bessho Y, Katoh K, Ookawara S, Fujioka M, Guillemot F & Kageyama R 2004. Hes genes regulate size, shape and histogenesis of the nervous system by control of the timing of neural stem cell differentiation. Development, 131, 5539–50. [PubMed: 15496443]

Heinz S, Benner C, Spann N, Bertolino E, Lin YC, Laslo P, Cheng JX, Murre C, Singh H & Glass CK 2010. Simple combinations of lineage-determining transcription factors prime cis-regulatory elements required for macrophage and B cell identities. Mol Cell, 38, 576–89. [PubMed: 20513432]

Hirata H, Bessho Y, Kokubu H, Masamizu Y, Yamada S, Lewis J & Kageyama R 2004. Instability of Hes7 protein is crucial for the somite segmentation clock. Nat Genet, 36, 750–4. [PubMed: 15170214]

Hirata H, Tomita K, Bessho Y & Kageyama R 2001. Hes1 and Hes3 regulate maintenance of the isthmic organizer and development of the mid/hindbrain. EMBO J, 20, 4454–66. [PubMed: 11500373]

Holley SA, Julich D, Rauch GJ, Geisler R & Nusslein-Volhard C 2002. her1 and the notch pathway function within the oscillator mechanism that regulates zebrafish somitogenesis. Development, 129, 1175–83. [PubMed: 11874913]

Hong CS & Saint-Jeannet JP 2018. The b-HLH transcription factor Hes3 participates in neural plate border formation by interfering with Wnt/beta-catenin signaling. Dev Biol, 442, 162–172. [PubMed: 30016640]

Horstick EJ, Jordan DC, Bergeron SA, Tabor KM, Serpe M, Feldman B & Burgess HA 2015. Increased functional protein expression using nucleotide sequence features enriched in highly expressed genes in zebrafish. Nucleic Acids Res, 43, e48. [PubMed: 25628360]

Hsu JY, Danis EP, Nance S, O'brien JH, Gustafson AL, Wessells VM, Goodspeed AE, Talbot JC, Amacher SL, Jedlicka P, Black JC, Costello JC, Durbin AD, Artinger KB & Ford HL 2022. SIX1 reprograms myogenic transcription factors to maintain the rhabdomyosarcoma undifferentiated state. Cell Rep, 38, 110323. [PubMed: 35108532]

Iuchi S & Kuldell N 2005. Zinc finger proteins from atomic contact to cellular function. Molecular biology intelligence unit Kluwer Academic/Plenum Publishers.

Jouve C, Palmeirim I, Henrique D, Beckers J, Gossler A, Ish-Horowicz D & Pourquie O 2000. Notch signalling is required for cyclic expression of the hairy-like gene HES1 in the presomitic mesoderm. Development, 127, 1421–9. [PubMed: 10704388]

Kageyama R, Ohtsuka T & Kobayashi T 2008. Roles of Hes genes in neural development. Dev Growth Differ, 50 Suppl 1, S97–103. [PubMed: 18430159]

Kendall GC & Amatruda JF 2016. Zebrafish as a Model for the Study of Solid Malignancies. In: KAWAKAMI K, PATTON EE & ORGER M (eds.) Zebrafish: Methods and Protocols New York, NY: Springer New York.

Kendall GC, Watson S, Xu L, Lavigne CA, Murchison W, Rakheja D, Skapek SX, Tirode F, Delattre O & Amatruda JF 2018. PAX3-FOXO1 transgenic zebrafish models identify HES3 as a mediator of rhabdomyosarcoma tumorigenesis. Elife, 7.

Kim D, Paggi JM, Park C, Bennett C & Salzberg SL 2019. Graph-based genome alignment and genotyping with HISAT2 and HISAT-genotype. Nat Biotechnol, 37, 907–915. [PubMed: 31375807]

Kingsbury TJ, Kim M & Civin CI 2019. Regulation of cancer stem cell properties by SIX1, a member of the PAX-SIX-EYA-DACH network. Adv Cancer Res, 141, 1–42. [PubMed: 30691681]

Li H, Handsaker B, Wysoker A, Fennell T, Ruan J, Homer N, Marth G, Abecasis G, Durbin R & Genome Project Data Processing, S. 2009. The Sequence Alignment/Map format and SAMtools. Bioinformatics, 25, 2078–9. [PubMed: 19505943]

Liao Y, Smyth GK & Shi W 2014. featureCounts: an efficient general purpose program for assigning sequence reads to genomic features. Bioinformatics, 30, 923–30. [PubMed: 24227677]

Ligon KL, Alberta JA, Kho AT, Weiss J, Kwaan MR, Nutt CL, Louis DN, Stiles CD & Rowitch DH 2004. The oligodendroglial lineage marker OLIG2 is universally expressed in diffuse gliomas. J Neuropathol Exp Neurol, 63, 499–509. [PubMed: 15198128]

Malone CM, Domaschenz R, Amagase Y, Dunham I, Murai K & Jones PH 2011. Hes6 is required for actin cytoskeletal organization in differentiating C2C12 myoblasts. Exp Cell Res, 317, 1590–602. [PubMed: 21501606]

Martin TA, Goyal A, Watkins G & Jiang WG 2005. Expression of the transcription factors snail, slug, and twist and their clinical significance in human breast cancer. Ann Surg Oncol, 12, 488–96. [PubMed: 15864483]

Masjkur J, Arps-Forker C, Poser SW, Nikolakopoulou P, Toutouna L, Chenna R, Chavakis T, Chatzigeorgiou A, Chen LS, Dubrovska A, Choudhary P, Uphues I, Mark M, Bornstein SR & Androutsellis-Theotokis A 2014. Hes3 is expressed in the adult pancreatic islet and regulates gene expression, cell growth, and insulin release. J Biol Chem, 289, 35503–16. [PubMed: 25371201]

Muller M, V Weizsacker E & Campos-Ortega JA 1996. Expression domains of a zebrafish homologue of the Drosophila pair-rule gene hairy correspond to primordia of alternating somites. Development, 122, 2071–8. [PubMed: 8681788]

Nagase H, Visse R & Murphy G 2006. Structure and function of matrix metalloproteinases and TIMPs. Cardiovasc Res, 69, 562–73. [PubMed: 16405877]

Oates AC & Ho RK 2002. Hairy/E(spl)-related (Her) genes are central components of the segmentation oscillator and display redundancy with the Delta/Notch signaling pathway in the formation of anterior segmental boundaries in the zebrafish. Development, 129, 2929–46. [PubMed: 12050140]

Ohtsuka T, Ishibashi M, Gradwohl G, Nakanishi S, Guillemot F & Kageyama R 1999. Hes1 and Hes5 as notch effectors in mammalian neuronal differentiation. EMBO J, 18, 2196–207. [PubMed: 10205173]

Onichtchouk D, Geier F, Polok B, Messerschmidt DM, Mossner R, Wendik B, Song S, Taylor V, Timmer J & Driever W 2010. Zebrafish Pou5f1-dependent transcriptional networks in temporal control of early development. Mol Syst Biol, 6, 354. [PubMed: 20212526]

Parham DM & Ellison DA 2006. Rhabdomyosarcomas in adults and children: an update. Arch Pathol Lab Med, 130, 1454–65. [PubMed: 17090187]

Park DM, Jung J, Masjkur J, Makrogkikas S, Ebermann D, Saha S, Rogliano R, Paolillo N, Pacioni S, Mckay RD, Poser S & Androutsellis-Theotokis A 2013. Hes3 regulates cell number in cultures from glioblastoma multiforme with stem cell characteristics. Sci Rep, 3, 1095. [PubMed: 23393614]

Pingault V, Zerad L, Bertani-Torres W & Bondurand N 2022. SOX10: 20 years of phenotypic plurality and current understanding of its developmental function. J Med Genet, 59, 105–114. [PubMed: 34667088]

Poser SW, Park DM & Androutsellis-Theotokis A 2013. The STAT3-Ser/Hes3 signaling axis: an emerging regulator of endogenous regeneration and cancer growth. Front Physiol, 4, 273. [PubMed: 24101906]

Poser SW, Park DM & Androutsellis-Theotokis A 2014. The STAT3-Ser/Hes3 signaling axis in cancer. Front Biosci (Landmark Ed), 19, 718–26. [PubMed: 24389215]

Prykhozhij SV, Steele SL, Razaghi B & Berman JN 2017. A rapid and effective method for screening, sequencing and reporter verification of engineered frameshift mutations in zebrafish. Dis Model Mech, 10, 811–822. [PubMed: 28280001]

Raghavan SS, Mooney KL, Folpe AL & Charville GW 2019. OLIG2 is a marker of the fusion protein-driven neurodevelopmental transcriptional signature in alveolar rhabdomyosarcoma. Hum Pathol, 91, 77–85. [PubMed: 31299267]

Robinson MD, Mccarthy DJ & Smyth GK 2010. edgeR: a Bioconductor package for differential expression analysis of digital gene expression data. Bioinformatics, 26, 139–40. [PubMed: 19910308]

Rojas-Rivera D, Armisen R, Colombo A, Martinez G, Eguiguren AL, Diaz A, Kiviluoto S, Rodriguez D, Patron M, Rizzuto R, Bultynck G, Concha ML, Sierralta J, Stutzin A & Hetz C 2012. TMBIM3/GRINA is a novel unfolded protein response (UPR) target gene that controls apoptosis through the modulation of ER calcium homeostasis. Cell Death Differ, 19, 1013–26. [PubMed: 22240901]

Sasai Y, Kageyama R, Tagawa Y, Shigemoto R & Nakanishi S 1992. Two mammalian helix-loop-helix factors structurally related to Drosophila hairy and Enhancer of split. Genes Dev, 6, 2620–34. [PubMed: 1340473]

Shankaran SS, Sieger D, Schroter C, Czepe C, Pauly MC, Laplante MA, Becker TS, Oates AC & Gajewski M 2007. Completing the set of h/E(spl) cyclic genes in zebrafish: her12 and her15 reveal novel modes of expression and contribute to the segmentation clock. Dev Biol, 304, 615–32. [PubMed: 17274976]

Sieger D, Ackermann B, Winkler C, Tautz D & Gajewski M 2006. her1 and her13.2 are jointly required for somitic border specification along the entire axis of the fish embryo. Dev Biol, 293, 242–51. [PubMed: 16545363]

Sieger D, Tautz D & Gajewski M 2004. her11 is involved in the somitogenesis clock in zebrafish. Dev Genes Evol, 214, 393–406. [PubMed: 15309634]

Sunkel BD, Wang M, Lahaye S, Kelly BJ, Fitch JR, Barr FG, White P & Stanton BZ 2021. Evidence of pioneer factor activity of an oncogenic fusion transcription factor. iScience, 24, 102867. [PubMed: 34386729]

Talbot JC & Amacher SL 2014. A streamlined CRISPR pipeline to reliably generate zebrafish frameshifting alleles. Zebrafish, 11, 583–5. [PubMed: 25470533]

Thisse C & Thisse B 2005. High Throughput Expression Analysis of ZF-Models Consortium Clones. ZFIN Direct Data Submission

Wang R, Chen F, Chen Q, Wan X, Shi M, Chen AK, Ma Z, Li G, Wang M, Ying Y, Liu Q, Li H, Zhang X, Ma J, Zhong J, Chen M, Zhang MQ, Zhang Y, Chen Y & Zhu D 2022. MyoD is a 3D genome structure organizer for muscle cell identity. Nat Commun, 13, 205. [PubMed: 35017543]

Wang Y, Weng X, Wang L, Hao M, Li Y, Hou L, Liang Y, Wu T, Yao M, Lin G, Jiang Y, Fu G, Hou Z, Meng X, Lu J & Wang J 2018. HIC1 deletion promotes breast cancer progression by activating tumor cell/fibroblast crosstalk. J Clin Invest, 128, 5235–5250. [PubMed: 30204129]

Wickham H, Averick M, Bryan J, Chang W, Mcgowan L, François R, Grolemund G, Hayes A, Henry L, Hester J, Kuhn M, Pedersen T, Miller E, Bache S, Müller K, Ooms J, Robinson D, Seidel D, Spinu V, Takahashi K, Vaughan D, Wilke C, Woo K & Yutani H 2019. Welcome to the Tidyverse. Journal of Open Source Software, 4.

Wickramasinghe CM, Domaschenz R, Amagase Y, Williamson D, Missiaglia E, Shipley J, Murai K & Jones PH 2013. HES6 enhances the motility of alveolar rhabdomyosarcoma cells. Exp Cell Res, 319, 103–12. [PubMed: 22982728]

Zhai G, Song J, Shu T, Yan J, Jin X, He J & Yin Z 2017. LRH-1 senses signaling from phosphatidylcholine to regulate the expansion growth of digestive organs via synergy with Wnt/beta-catenin signaling in zebrafish. J Genet Genomics, 44, 307–317. [PubMed: 28642062]

Highlights

- Generated zebrafish *her3* CRISPR/Cas9 knockouts with loss-of-function mutations
- *her3* mutant is unable to bind known target, neurog1, causing dysregulated expression
- *her3* loss causes abnormal expression of core subset of developmental regulatory genes
- Sox10 DNA binding motifs enriched in *her3* knockout differentially expressed genes
- Tumor microenvironment and matrix metalloprotease pathways are enriched in *her3* knockout

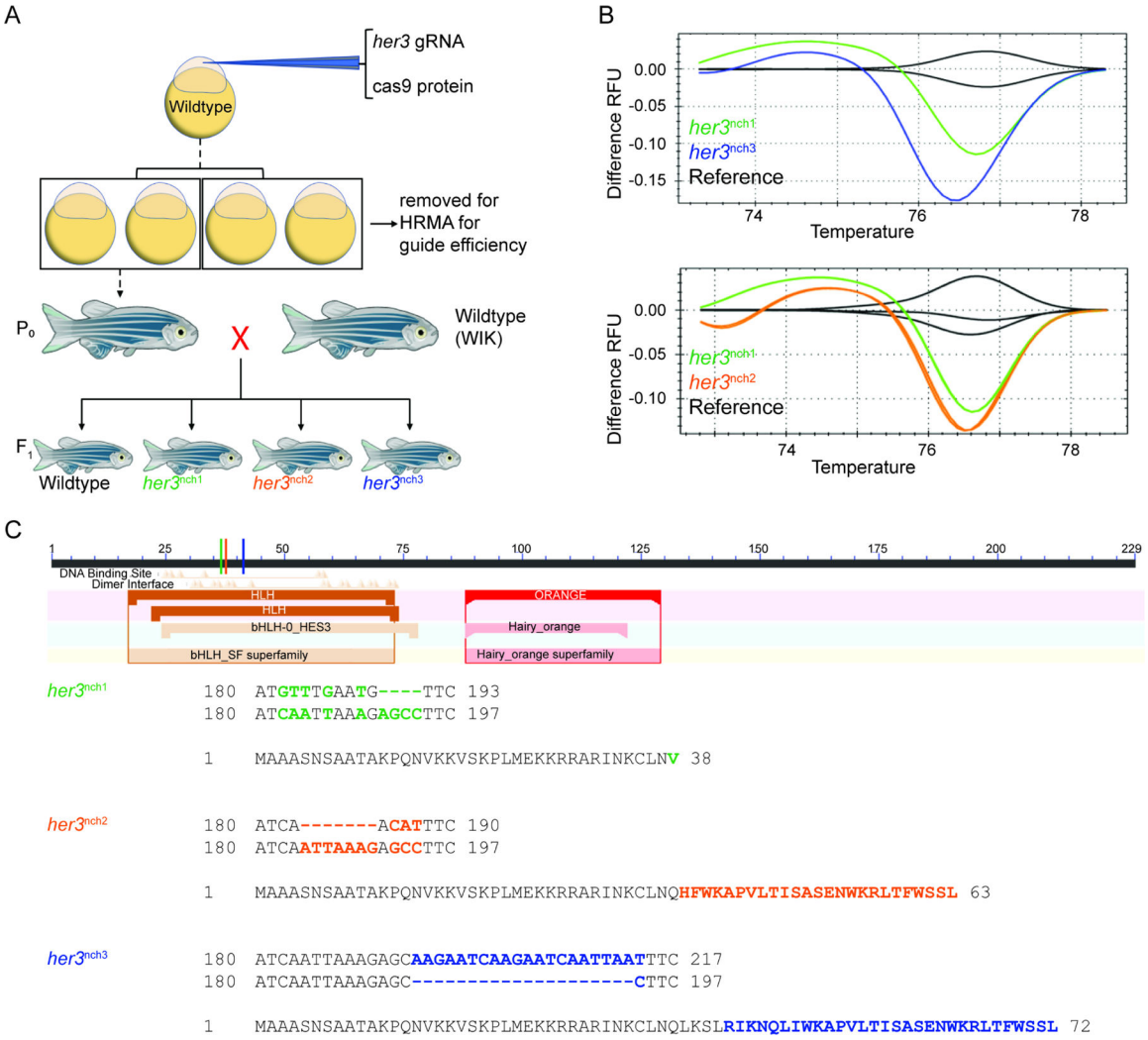

Figure 1: Generating *her3* mutations in zebrafish.

(A) Schematic of strategy to generate a *her3* CRISPR/Cas9 null mutant zebrafish. Zebrafish embryos were injected in the cytoplasm at the 1-cell stage with both Cas9 protein and *her3* gRNA. A subset of the injected clutch was set aside to determine gRNA efficiency. The remaining embryos were grown up to identify adult founders, which were outcrossed to wildtype WIK zebrafish to generate the F_1 generation. (B) HRMA difference RFU graphs of F_1 heterozygous zebrafish generated from three identified founders. Fin clips of adult F_1 zebrafish were taken and HRMA was performed to identify potential mutations, with different melt curves indicating distinct DNA mutations. Wildtype reference fish are labeled black, *her3*^{nch1} fish are labeled green, *her3*^{nch2} fish are labeled orange, and *her3*^{nch3} fish are labeled blue. Each line represents an individual fish. (C) Schematic of full length Her3 protein and identified mutation sequences. To determine the mutation sequence, the *her3* gRNA target site from the three prospective mutant F_1 fish was A-tail cloned into the pGEM T-Easy vector. Multiple colonies from each line were Sanger sequenced with an SP6 primer. The mutated sequence was then aligned with the wildtype reference sequence for *her3.* Colored lines in the schematic indicate where the predicted frameshift mutation occurs for

each respective mutation, all of which are in the DNA binding domain. Below, the DNA sequence and amino acid sequence are shown for the three mutations, with mutant DNA sequence on top of the aligned wildtype sequence. For both the DNA sequence and the amino acid sequence, colored and bolded letters highlight the mutated sequence.

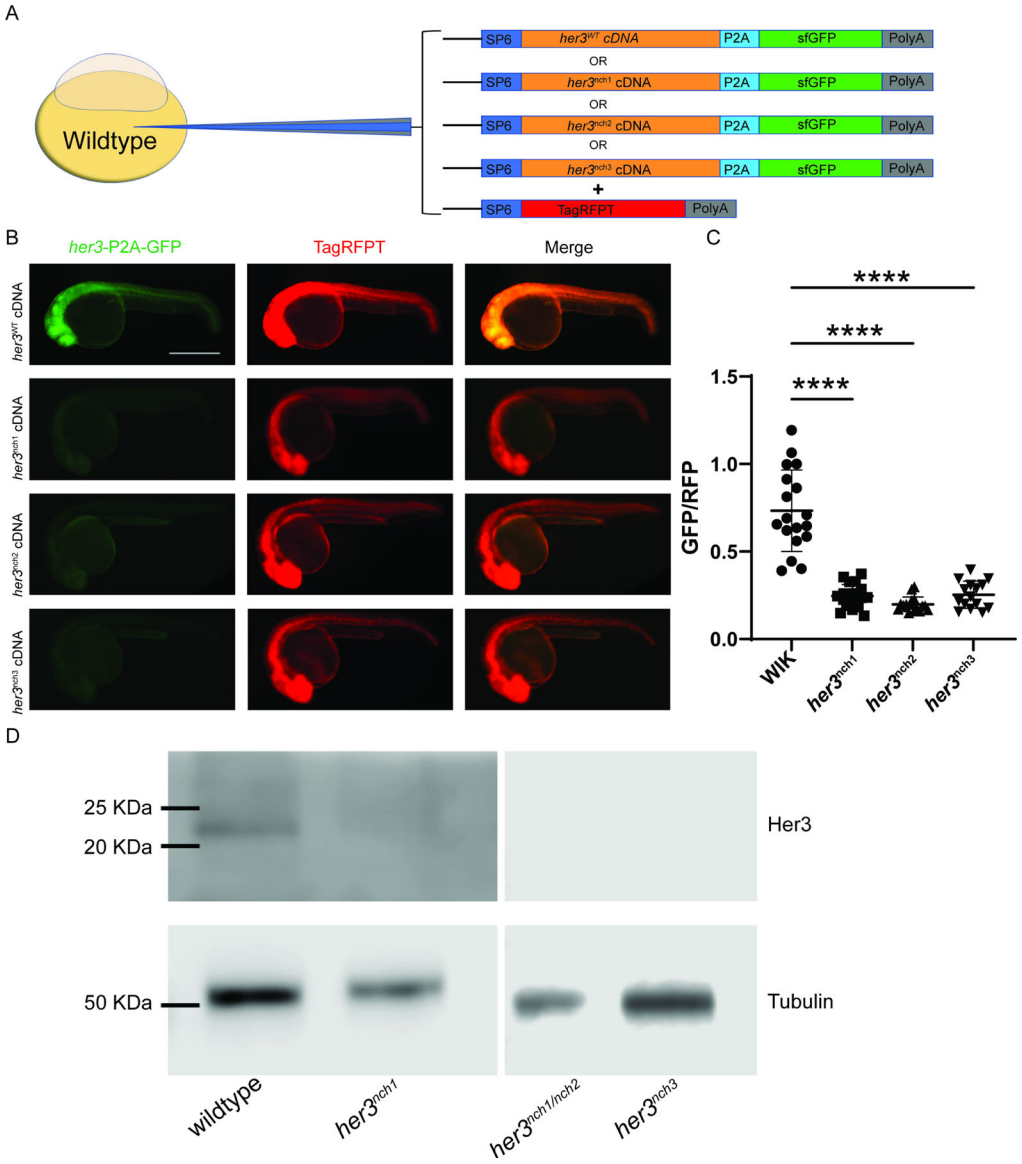

Figure 2: Validating *her3* frameshift mutations.

(A) Schematic of strategy for *her3* mRNA expression assay. Zebrafish embryos were co-injected with a mixture of two different mRNAs: one of four different *her3*-P2A-sfGFP generated from either wildtype *her3* or each of the three mutant *her3* zebrafish; and a control TagRFPT mRNA. mRNA mixtures were injected into the yolk of zebrafish embryos at the 1–4 cell stage (see Figure S5 for sequences). (B) At 24 hours post fertilization (hpf), embryos were imaged on a Leica M205FA fluorescent microscope to quantify GFP and RFP fluorescence. GFP fluorescence indicates either the *her3* wildtype or *her3* mutant P2A-sfGFP construct, whereas TagRFPT is an injection control. Scale bar is 500μm. (C) Plotted is the raw integrated density ratio of GFP to RFP fluorescence. Each mark represents an individual fish. Wildtype (WIK): n=18. nch1: n=19. nch2: n=16. nch3: n=15. A Brown-Forsythe and Welch ANOVA was performed with Dunnett T3 multiple comparison test. The comparisons include wildtype WIK to *her3* mutants with the following P values: WIK-

her3^{nch1}: p=1.20×10^{-7}. WIK- *her3*^{nch2}: p=5.24×10^{-8}. WIK- *her3*^{nch3}: p=1.60×10^{-7}. (D) Western blot of 6hpf embryos from *her3*^{nch1} and *her3*^{nch3} homozygotes, and a compound heterozygote for *her3*$^{nch1/nch2}$. A cross-reactive human HES3 antibody was used to detect zebrafish wildtype Her3, and a Tubulin antibody was used as a loading control.

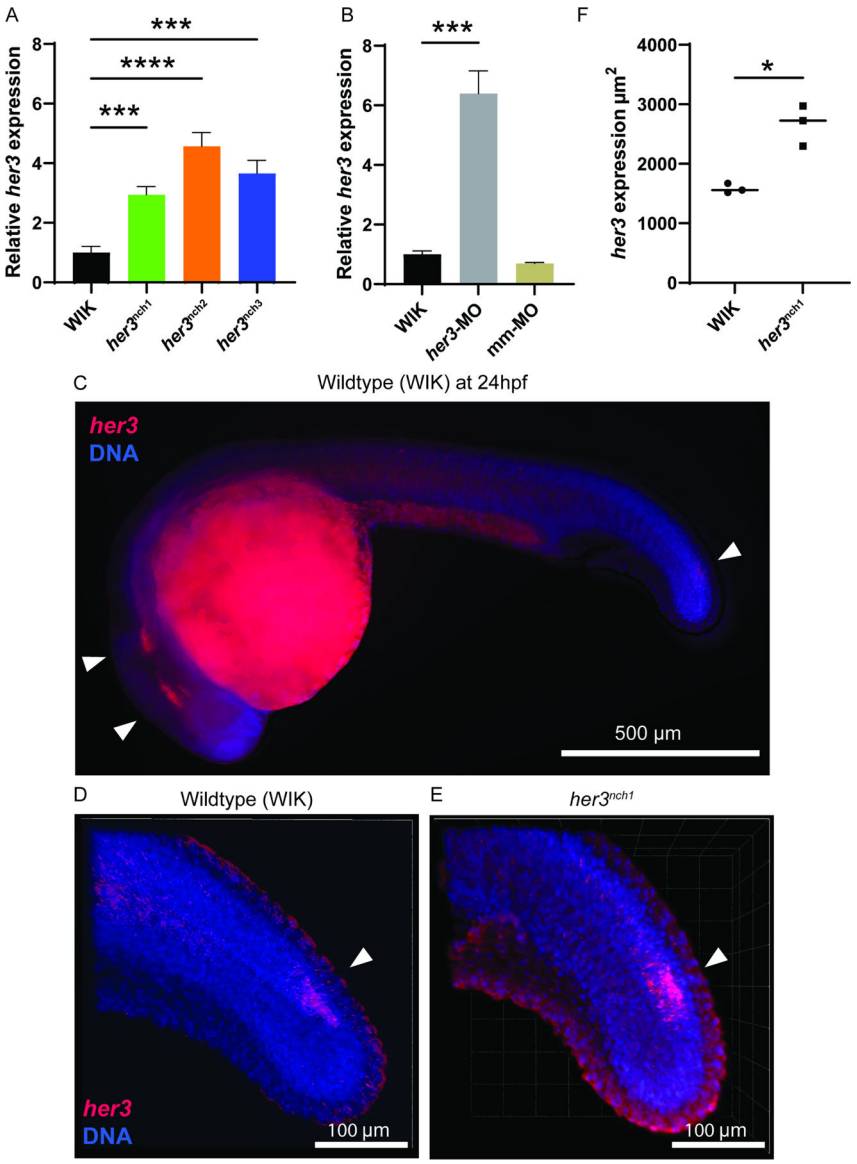

Figure 3: *her3* null mutation recapitulates *her3*-morpholino phenotype.

(A) qRT-PCR for *her3* from each *her3* null mutant line compared to the wildtype WIK. qRT-PCR was done with 3 biological replicates per line, with each replicate containing a pool of 10, 24hpf embryos. Each biological replicate is comprised of three technical replicates. Statistical significance was determined by a one way ANOVA with Dunnett multiple comparison test. WIK- *her3*^{nch1}: $p=1.82\times10^{-3}$. WIK- *her3*^{nch2}: $p<1.00\times10^{-4}$. WIK-*her3*^{nch3}: $p<1.00\times10^{-4}$. (B) qRT-PCR for *her3* with WIK, *her3*-MO, and mismatch (mm)-MO. 5–10nL of morpholinos at a concentration of 500µM were injected into the yolk of WIK embryos at the 1–4 cell stage. qPCR was done with 3 biological replicates per condition, with each replicate containing a pool of 10, 24hpf embryos. Each biological replicate is comprised of three technical replicates. Statistical significance was determined by a one way ANOVA with Dunnett multiple comparison test. WIK-*her3*-MO: $p<1.0\times10^{-4}$. WIK-mm-MO: $p=8.46\times10^{-1}$, not significant. (C) RNAscope on whole mount 24hpf WIK

wildtype zebrafish embryos. RNAscope targeting *her3* RNA transcripts (red) was done and counterstained with DAPI (blue). Representative image was taken on a Leica M205FA fluorescent stereoscope out of three embryos evaluated. Scale bar is 500μm. (D-E) RNAscope targeting *her3* RNA transcripts was done on 24hpf WIK (D) and 24hpf *her3*^{nch1} (E) embryos and counterstained with DAPI. Images were taken on a Zeiss LSM800 confocal microscope with a 20x objective. Images shown are z-stack projections: (D) WIK is a projection of 53, 2μm slices; (E) *her3*^{nch1} is a projection of 48, 2μm slices. *her3* is shown in red and DAPI is shown in blue. (F) Quantification of the area of *her3* expression from (D-E) indicated by white arrowheads. WIK and *her3*^{nch1}: n=3 embryos per condition. A Welch's two-tailed t-test had a p-value of 2.62×10^{-2}.

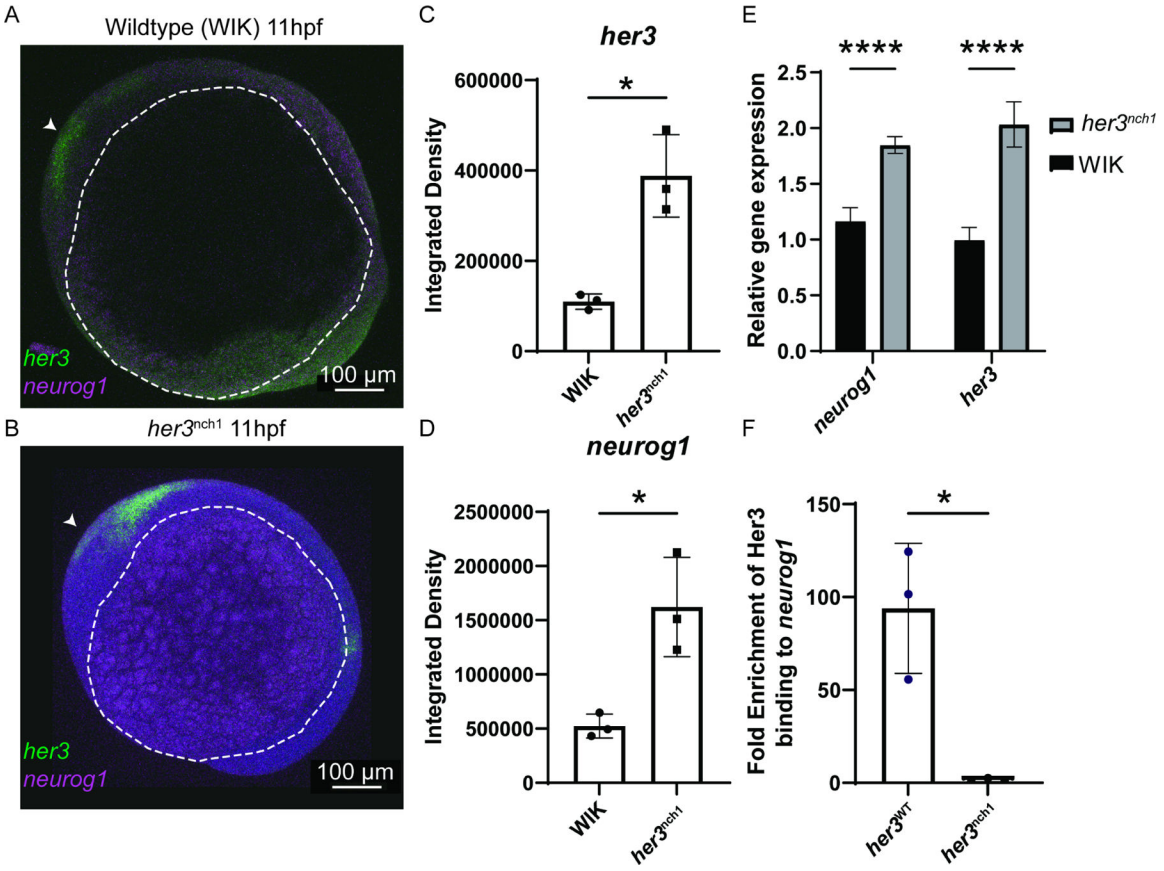

Figure 4. *her3* null mutation results in deregulation of *neurog1* expression.

(A-B) RNAscope confocal images of *her3* (green) and *neurog1* (purple) in 11hpf WIK (A) and 11hpf *her3*^{nch1} homozygous (B) embryos. White arrowhead denotes anterior of the embryo. White dotted line outlines the yolk of the embryos. (C-D) Integrated density of the *her3* (C) and *neurog1* (D) expression are quantified. Both WIK and *her3*^{nch1}: n=3 samples per condition. Statistical significance was determined by a Welch's two-tailed t-test. *her3*: p=0.0306. *neurog1*: p=0.0470. (E) qRT-PCR for *neurog1* and *her3* using 11hpf WIK and *her3*^{nch1} embryos. qRT-PCR includes four biological replicates per line, with each replicate containing a pool of 40, 11hpf embryos. Each biological replicate is comprised of three technical replicates. Statistical significance was determined by an unpaired Welch's t-test. *neurog1* p=2.11×10^{-4}. *her3* p=4.14×10^{-4}. (F) ChIP-qPCR using 6hpf WIK embryos injected with FLAG-tagged *her3* mRNA cloned from either wildtype WIK zebrafish or *her3*^{nch1} zebrafish. For each mRNA injected, n=3 biological replicates are shown from independent experiments. For each sample, one million zebrafish cells were combined with one million Rh30 cells (human rhabdomyosarcoma cell line) as carrier chromatin. After FLAG ChIP for the wildtype Her3 or Her3^{nch1} mutant construct, qPCR was performed targeting known Her3 binding sites in the *neurog1* promoter. Fold enrichment was calculated by comparing FLAG tagged Her3 or Her3^{nch1} mutant binding in the *neurog1* promoter as compared to a gene desert. Statistical significance (p=4.46×10^{-2}) was calculated using an unpaired Welch's t-test.

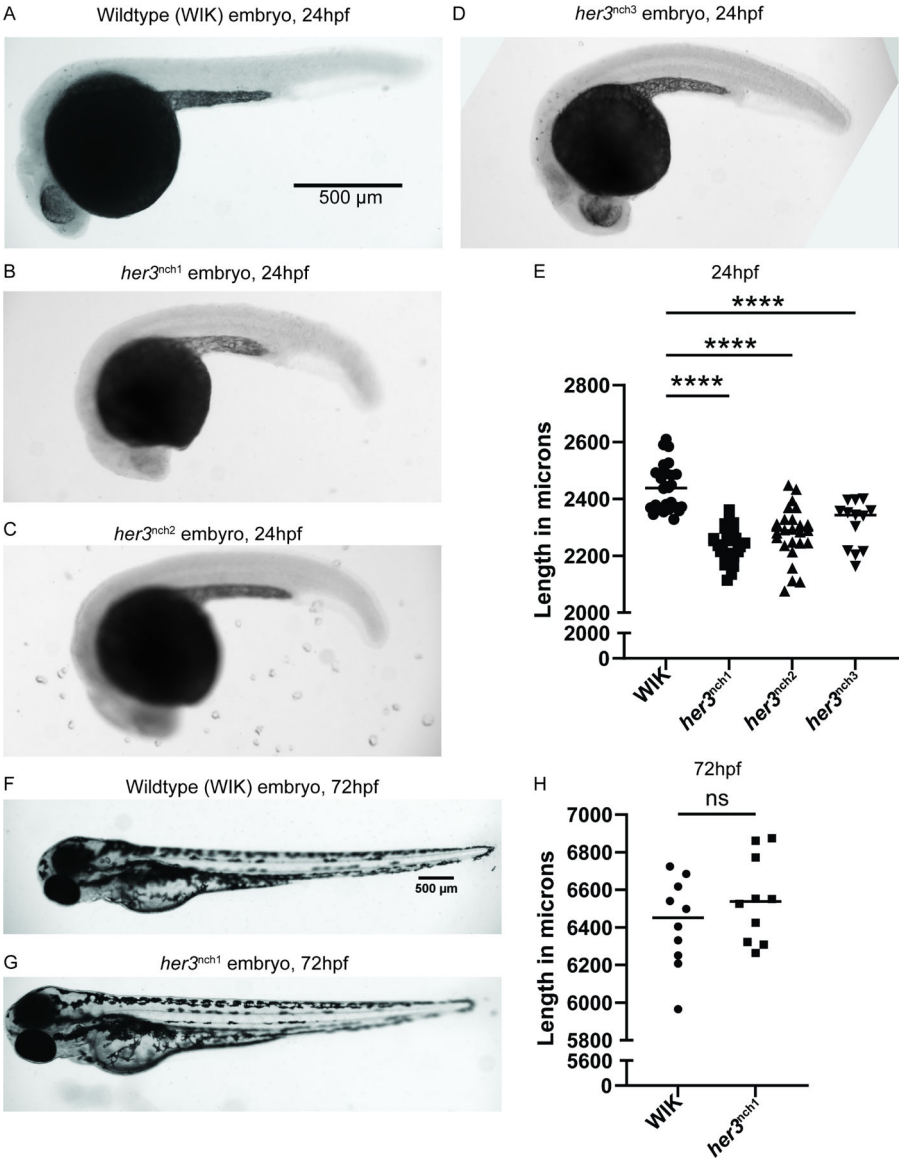

Figure 5: *her3* null mutant lines are significantly smaller than wildtype WIK at 24hpf.

(A-D) Brightfield images of 24hpf wildtype WIK (A), 24hpf *her3*^{nch1} (B), 24hpf *her3*^{nch2} (C), and 24hpf *her3*^{nch3} (D) embryos. Images were taken on a Leica M205FA fluorescent stereoscope. Scale bar is 500µm. (E) The standard length of each embryo was measured and graphed here. WIK: n=28. *her3*^{nch1}: n=25. *her3*^{nch2}: n=25. *her3*^{nch3}: n=13. For each comparison to WIK, $p<1.00\times10^{-4}$ using a one-way ANOVA with Dunnett test. (F-G) Brightfield images of 72hpf wildtype WIK (F) and 72hpf *her3*^{nch1} (G) embryos. (H) The standard length of each 72hpf embryo was also measured and graphed here. n=10 for both WIK and *her3*^{nch1}. Each point is an individual fish. An unpaired Welch's t-test indicated this comparison was not statistically significant.

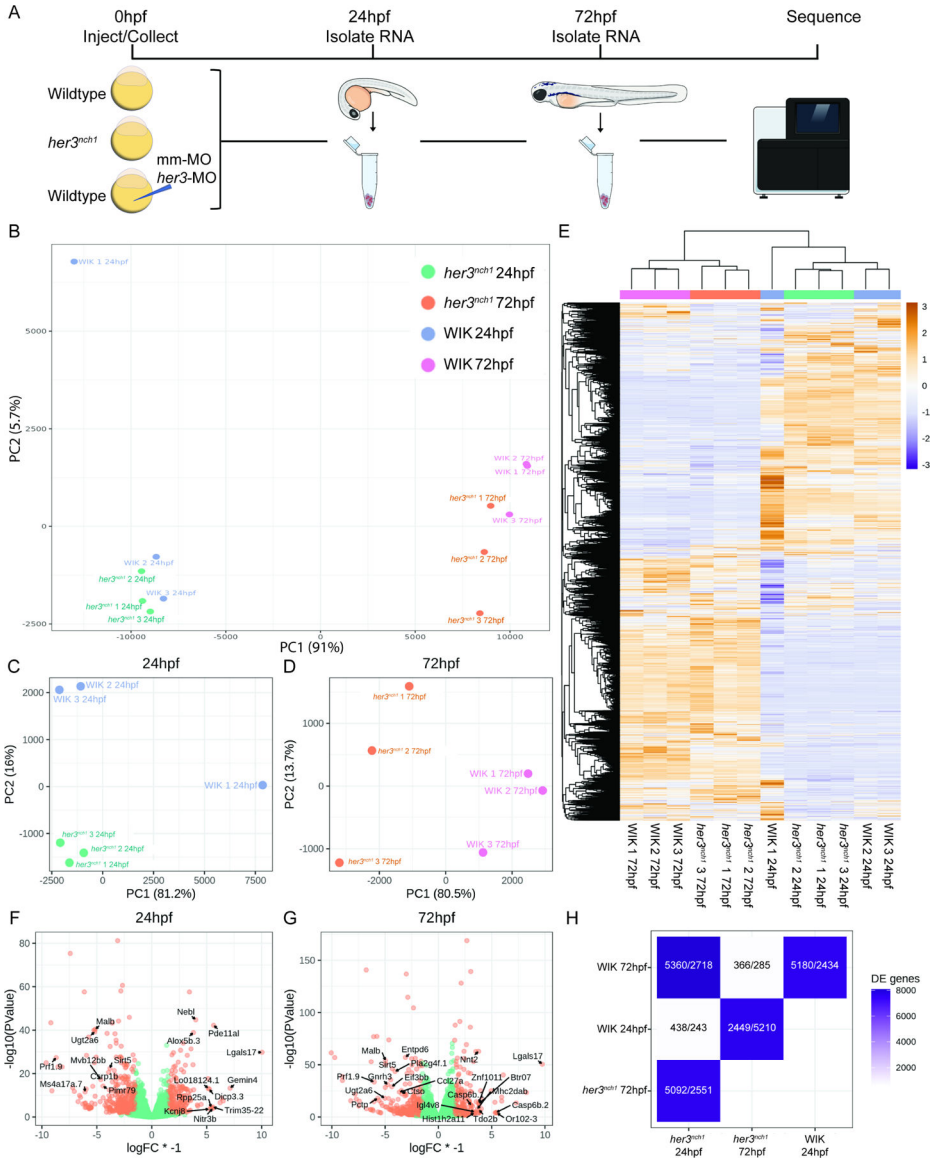

Figure 6: Transcriptional impact of *her3* mutation status.

(A) Schematic of RNA collection. Embryos from wildtype WIK in-cross and *her3*^{nch1} in-cross were collected, with a subset of WIK embryos injected with either *her3*-MO or mismatch-MO. At 24hpf, RNA was isolated from 3 groups of 25 embryos each per condition, and again at 72hpf. RNA was then sent for sequencing. (B) PCA of all samples, excluding MO samples. (C-D) PCA of *her3*^{nch1} and WIK 24hpf samples (C) and 72hpf samples (D). (E) Heatmap clustering of all differentially expressed genes from *her3*^{nch1} and WIK samples. (F-G) Volcano plots of differentially expressed genes in *her3*^{nch1} compared to WIK 24hpf samples (F) and 72hpf samples (G). Differential expression was considered significant with an FDR ≤ 0.1 and absolute value of logFC ≥ 1.5. Top annotated up- and downregulated genes are labeled. (H) Tile chart showing pairwise comparisons of differentially expressed genes. Numbers are displayed as downregulated/upregulated of the groups along the x-axis.

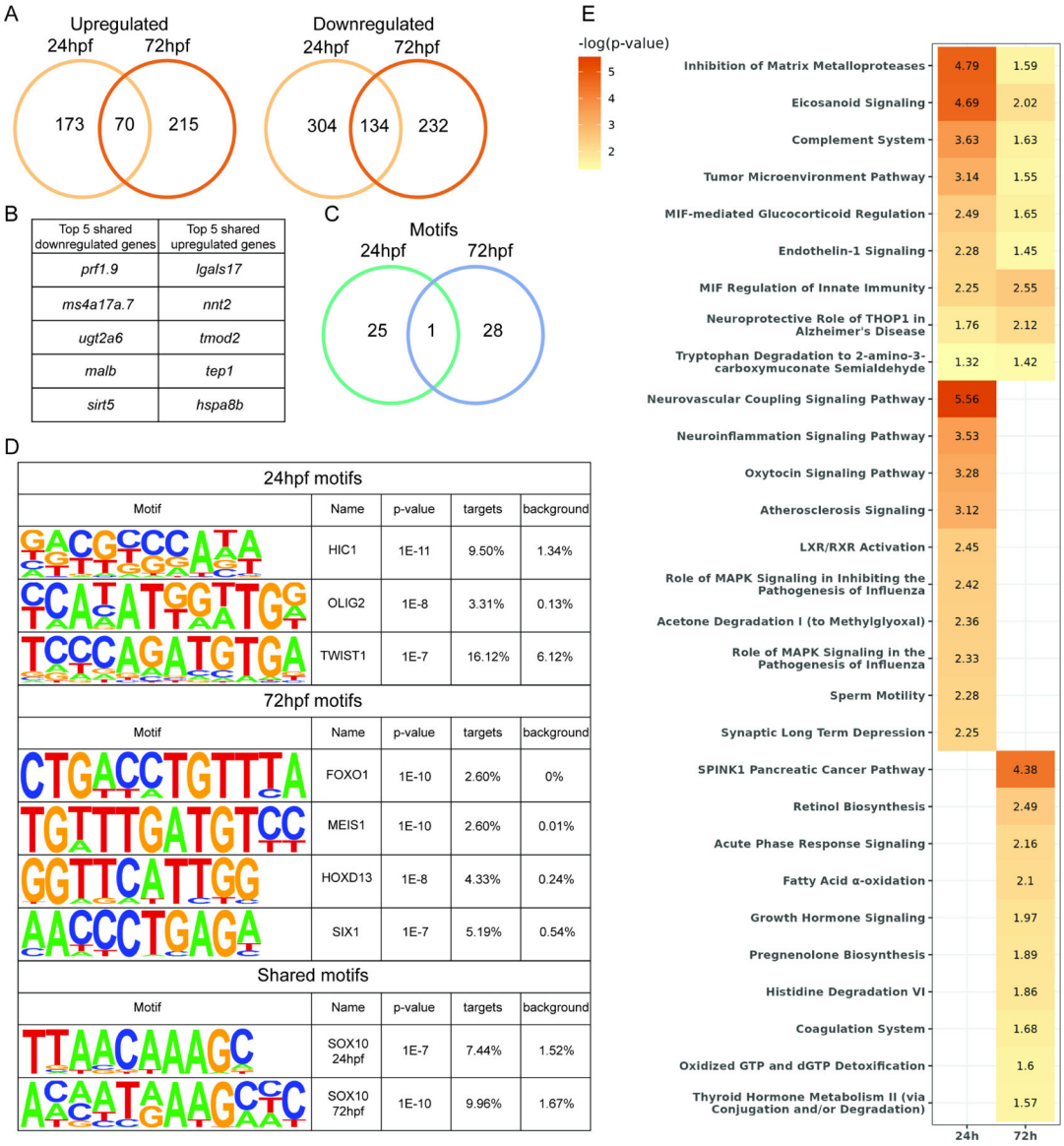

Figure 7: Development and cancer genes and pathways are impacted by *her3* null mutation.

(A) Venn diagram showing overlap of differentially expressed genes from *her3* null mutant between 24hpf and 72hpf embryos. (B) List of the top 5 up- and downregulated genes shared between 24hpf and 72hpf in the *her3* null mutant. (C) Venn diagram of transcription factors with DNA binding motifs overlapping between 24hpf and 72hpf *her3* null mutant embryos. Targets are the percentage of differentially expressed genes that contain the motif. Background is the percentage of non-differentially expressed genes that contain the motif. (D) Examples of motifs from Venn diagram in (C). (E) p-value chart showing IPA pathways that are significantly enriched with identified differentially expressed genes.